PCCP

PAPER

View Article Online
View Journal | View Issue

Cite this: *Phys. Chem. Chem. Phys.*, 2018, **20**, 25910

Ultrafast unidirectional chiral rotation in the *Z–E* photoisomerization of two azoheteroarene photoswitches†

Xiaojuan Pang,[a] Chenwei Jiang,*[a] Yongnan Qi,[a] Ling Yuan,[a] Deping Hu,[b] Xiuxing Zhang,[c] Di Zhao,[a] Dongdong Wang,[d] Zhenggang Lan*[b] and Fuli Li[a]

Received 26th July 2018,
Accepted 16th September 2018

DOI: 10.1039/c8cp04762f

rsc.li/pccp

Unidirectional rotation represents a very important functional feature in photochemistry, such as in the design of light-driven molecular rotary motors. Great attention has recently been devoted to the unidirectional preference of the torsional motion of azobenzene and other molecules. Azoheteroarenes offer functional advantages over their more conventional azobenzene counterparts due to the introduction of heteroaromatic rings. In this paper, the *Z–E* photoisomerization dynamics of two azoheteroarenes, 1,2-bis(1-methyl-1*H*-imidazol-2-yl)diazene and 1,2-bis(1*H*-imidazol-2-yl)diazene, are investigated with trajectory surface-hopping molecular dynamics at the semi-empirical OM2/MRCI level. Starting from the S_1 excited state of the *M*-helical *Z*-isomer of both azoheteroarenes, more than 99% of the trajectories decay to their ground states through the *M*-helical conical intersections by twisting about the central N=N double bond. This chiral path preference can be well understood by the energy profiles generated by the linear interpolation between the Franck–Condon geometry of the *M*-helical *Z*-isomer and the relevant S_1/S_0 conical intersections. The *Z–E* photoisomerization mechanisms of these two azoheteroarenes display a higher preference for unidirectional rotary dynamics under a chiral path than their counterpart azobenzene.

1 Introduction

Owing to their potential applications in molecular switches and other devices, azobenzene and its derivatives have been widely studied both experimentally[1–17] and theoretically.[18–40] As a relatively new type of azobenzene derivative, azoheteroarenes, which represent a type of molecule in which one or two of the aryl rings from the conventional azobenzene class have been replaced with a five-membered heteroaromatic ring, have attracted increasing attention.[41–48]

Azoheteroarene photoswitches can offer functional advantages over their more conventional azobenzene counterparts due to the inclusion of their heteroaromatic rings. Azoheteroaryl photoswitches based on pyrroles and pyrazoles have been investigated by Weston *et al.*,[41] and their study clarified the dependence of their switching properties on the type, positioning, and substitution of the heteroaryl rings. Through heteroaryl design, a wide array of comparable azoheteroaryl photoswitches have recently been synthesized by Calbo *et al.*[42] In particular, a new azopyrazole named 3pzH, a type of azoheteroarene, has been found to be quantitatively switchable between its *Z* and *E* isomers with different wavelength irradiation, and it has a very long half-life (74 days at 25 °C) for thermal isomerization. The thermal *Z–E* isomerization mechanism of a class of five-membered photoswitchable azoheteroarenes was systematically investigated by Yin *et al.*[43] recently. Using first-principles density-functional calculations, a rotation-assisted inversion mechanism in the ground state was suggested.

Unidirectional rotation represents a very important feature in photochemistry, for example, in the movement of light-driven molecular rotary motors. Light-driven molecular rotary motors, based on the chiral crowded alkene designed by

[a] *Key Laboratory for Quantum Information and Quantum Optoelectronic Devices Shaanxi, and Department of Applied Physics, Xi'an Jiaotong University, Xi'an 710049, China. E-mail: jiangcw@xjtu.edu.cn*
[b] *Qingdao Institute of Bioenergy and Bioprocess Technology, Chinese Academy of Sciences, 189 Songling Road, Qingdao, 266101 Shandong, China. E-mail: lanzg@qibebt.ac.cn*
[c] *Department of Physics, Weinan Normal University, Weinan 714000, China*
[d] *Department of Applied Chemistry, School of Science, Xi'an Jiaotong University, Xi'an 710049, China*

† Electronic supplementary information (ESI) available: Detailed procedures of preparing excited state surface hopping molecular dynamics simulation; optimized geometries of both azoheteroarenes; distribution of geometrical parameters and reaction pathways for the *Z–E* photoisomerization of both azoheteroarenes; Cartesian coordinates for several structures of both azoheteroarenes; conical intersection structures related to the *Z–E* photoisomerization of azoheteroarene BHID. See DOI: 10.1039/c8cp04762f

Feringa and co-workers,[49–51] represent a group of promising molecular machines displaying unidirectional rotation. Some attention has recently been paid to the highly efficient unidirectional preference of the torsional motion of azobenzene and other molecules.[26,35,44,52] For the *cis*(*Z*)–*trans*(*E*) photoisomerization of azobenzene, a chiral path preference was observed by Weingart *et al.*[35] From the S_1 excited state of *P*-helical *cis*(*Z*)-azobenzene, about 77% of the trajectories decay from the channel that maintains the initial *P*-helicity, while about 22% of the trajectories decay along the *M*-helicity path. From an *ab initio* (CASSCF/STO-3G) surface hopping study, a similar chiral path selectivity in azobenzene was reported by Ootani *et al.*[26] Based on the Zhu–Nakamura theory,[53,54] with on-the-fly trajectory surface hopping simulations at the CASSCF level, Gao *et al.*[39] observed a chiral conversion pathway for the *cis–trans* photoisomerization of a bridged-azobenzene. Using a chiral rotary molecular motor model, which was a pentenylidene-pyrrolinium compound, Marchand *et al.*[52] predicted that the *Z–E* photoisomerization was more than 70% unidirectional (76% *vs.* 24% for clockwise and counter-clockwise rotation, respectively). By comparing the photoinduced isomerization mechanism of two arylazopyrazole photoswitches (1,3,5-trimethyl-4-(phenyldiazenyl)-1*H*-pyrazole and 1-methyl-4-(phenyldiazenyl)-1*H*-pyrazole), Wang *et al.*[44] observed a nearly stereospecific unidirectional (97% *vs.* 3%) excited-state relaxation for the *Z* isomer of 1,3,5-trimethyl-4-(phenyldiazenyl)-1*H*-pyrazole arising from the steric strain of methyl substitution. The question arises as to whether we can design a more general and efficient unidirectional excited-state torsional azoheteroarene system, *e.g.* without steric strain from the methyl group.

To the best of our knowledge, in most of the literature, azoheteroarenes have been designed by replacing one of the aryl rings in the azobenzene class with different five-membered heteroaromatic rings.[41–44] Very recently, a new azoheteroarene photoswitch, 1,2-bis(1-methyl-1*H*-imidazol-2-yl)diazene, was synthesized by Weston *et al.*,[45] in which both aryl rings in azobenzene are replaced with five-membered heteroaromatic ring imidazoles. When this azoheteroarene is protonated, the solution pH can be reversibly controlled owing to the significant difference in the acid dissociation constant pK_a values between its *E* and *Z* isomers. However, more unresolved questions exist regarding the photochemistry of azoheteroarenes. For instance, how can one modify the photochemical behavior by the inclusion of five-membered aromatic rings? How about the performance of this azoheteroarene as a photoswitch? And does the photoisomerization of these systems also display a similar preference in the chiral selectivity, as has been found in azobenzene? To answer these questions, the photoisomerization dynamics of this type of azoheteroarene should be investigated in detail.

In this study, using the trajectory surface-hopping molecular dynamics at the semi-empirical OM2/MRCI level, we systematically investigated the *Z–E* photoisomerization of two azoheteroarenes with two five-membered heteroaromatic rings, as shown in Scheme 1. A stereospecific unidirectional excited-state relaxation channel in both azoheteroarenes was found, which can be well understood by the energy profiles generated by the linear interpolation between the Franck–Condon geometry of the *Z*-isomer and the relevant S_1/S_0 conical intersections.

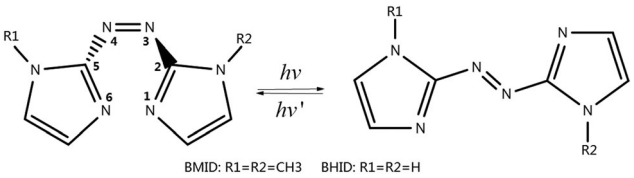

Scheme 1 Photoisomerization between *Z* and *E* isomers of the azoheteroarenes 1,2-bis(1-methyl-1*H*-imidazol-2-yl)diazene and 1,2-bis(1*H*-imidazol-2-yl)diazene (named BMID and BHID hereinafter, respectively). Several atoms in the central region are labelled.

The paper is organized as follows: in Section 2, we discuss the basic theoretical methods and the simulation details. The results of the *Z–E* photoisomerization dynamics of two azoheteroarenes are presented in Section 3. Finally, we summarize our results and discussion in Section 4.

2 Computational details

All electronic structure calculations were performed using the semi-empirical OM2/MRCI method as implemented in the development version of the MNDO program.[55] This method can provide a reasonable compromise between the computational cost and accuracy, as shown by many benchmark calculations,[56–61] and it has been successfully used in previous studies of many photo-induced processes.[35,36,44,62–65] The required energies, gradients, and nonadiabatic couplings were calculated analytically. The self-consistent field (SCF) calculations were performed in the closed-shell Hartree–Fock formalism for the ground state optimization. In the excited-state calculations, the molecular orbitals were obtained with the restricted open-shell Hartree–Fock (ROHF) formalism, as it provided a better orbital representation to construct the excited-state wave functions. Three reference configurations, including the closed-shell ground-state configurations combined with single and double excitations from the highest occupied molecular orbital (HOMO) to the lowest unoccupied molecular orbital (LUMO), were used to generate the multi-reference configuration interaction (MRCI) expansion.

The active space in the MRCI calculations included ten electrons in nine orbitals, which comprised four highest doubly occupied orbitals, two singly occupied orbitals and three lowest unoccupied orbitals. The geometries of the ground state S_0 minima were optimized at the OM2/MRCI level. For comparison, the ground state structures were also optimized at the B3LYP/6-311G(d,p) and CAM-B3LYP/6-311G(d,p) levels implemented using the GAUSSIAN 03 software package.[66] The optimization of the S_0/S_1 minimum-energy conical intersection (CI) structures was undertaken using the Lagrange-Newton[67] approach.

Surface hopping excited-state dynamics simulations were performed with Tully's fewest-switches algorithm.[68–70] An empirical decoherence correction (0.1 a.u.) proposed by Granucci *et al.*[71] was also used. Initial geometries and velocities were obtained using the Wigner sampling method.[72] The nuclear motion was

solved using the velocity Verlet algorithm with a constant time step of 0.1 fs, while the time-dependent electronic Schrödinger equation was propagated with a 100 times smaller time step.

We should emphasize that the initial sampling was also based on the S_0–S_1 transition probability of each geometry generated from the Wigner distribution function of the lowest vibrational level of the electronic ground state. The detailed procedures of preparing the excited state surface hopping molecular dynamics simulation for BMID and BHID are presented in the first part of the ESI.† Dynamics runs were initiated in the first singlet excited state. A total of 764 trajectories starting from the S_1 excited state of the *M*-helical *Z*-isomer of azoheteroarene BMID and 694 trajectories starting from the S_1 excited state of the *P*-helical *Z*-isomer of azoheteroarene BMID were calculated for 300 fs. While a total of 649 trajectories starting from the S_1 excited state of the *M*-helical *Z*-isomer of azoheteroarene BHID were also calculated for 300 fs. The definitions of *M* and *P* helicity in this paper are the same as those for *cis*(*Z*)-azobenzene[35] and *cis*(*Z*)-arylazopyrazole.[44]

3 Results and discussion

3.1 *Z*–*E* photoisomerization of azoheteroarene BMID

The optimized geometries of the *Z* and *E* isomers of azoheteroarene BMID using the OM2/MRCI method are presented in Fig. S1 and Table S1 (see the ESI†). For comparison, the corresponding geometrical values calculated with B3LYP/6-311G(d,p) and CAM-B3LYP/6-311G(d,p) using the GAUSSIAN 03 software package,[66] and cited from ref. 45, are also summarized in Table S1 (ESI†). As we can see, the optimized geometries obtained from the different methods above are consistent with each other.

At the end of our simulations, all 764 trajectories starting from the S_1 excited state of the *M*-helical *Z*-isomer of azoheteroarene BMID hopped to the ground state. A total of 360 trajectories experienced the *E*-isomer, so the *Z*–*E* photoisomerization quantum yield of BMID was estimated to be approximately 47%.

The time distribution of the $S_1 \rightarrow S_0$ hopping events of a total of 764 trajectories is presented in Fig. 1(a). The average occupation of the electronic states S_0 and S_1, together with the derivative of the S_0 population, as a function of simulation time is shown in the inset of Fig. 1(a). As we can see, the S_1 population decay was obviously not exponential. There was nearly no decay before 20 fs, after which, three major hopping event maxima arose at around 30, 50 and 100 fs, respectively. A similar relaxation pattern was also observed for the S_1 excited state relaxations of *cis*(*Z*)-azobenzene by Weingart *et al.*[35] and the *cis*(*Z*)-isomer of the arylazopyrazole 1,3,5-trimethyl-4-(phenyldiazenyl)-1*H*-pyrazole by Wang *et al.*[44] From the S_1 excited state lifetimes of all 764 trajectories, the average S_1 excited-state lifetime of the *M*-helical *Z*-isomer of azoheteroarene BMID was estimated to be approximately 54 fs.

In Fig. 1(a), the hopping events through the *M*-helical channel are separated from those through the *P*-helical channel by different colors. The hopping through the *M*-helical S_1/S_0 conical intersection is presented by the red bars, while that through the *P*-helical S_1/S_0 conical intersection is shown by blue bars. As we can see, almost all of the trajectories maintained their initial *M*-helicity, while only very few trajectories decayed through the *P*-helical channel.

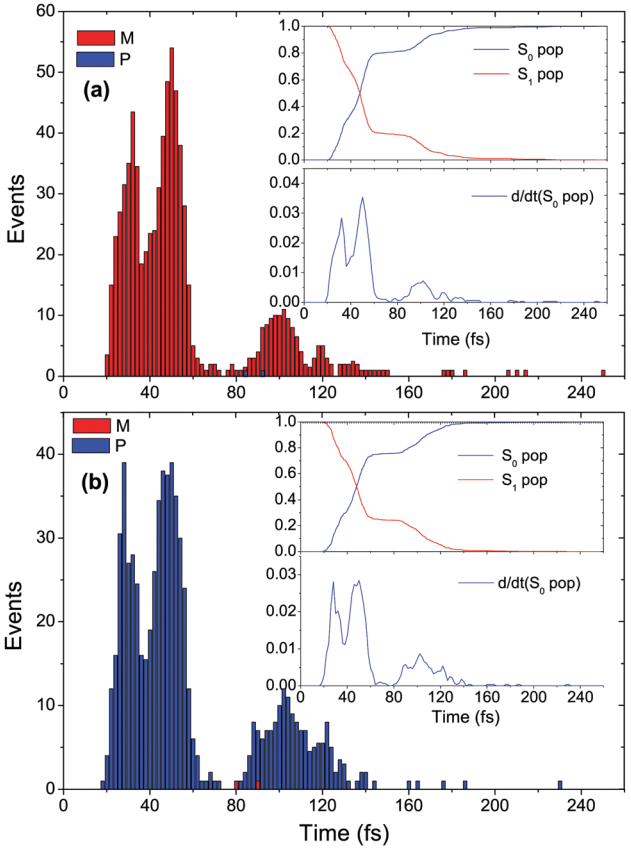

Fig. 1 Distributions of the $S_1 \rightarrow S_0$ hopping times of (a) 764 trajectories starting from the *M*-helical *Z*-isomer of azoheteroarene BMID and (b) 694 trajectories starting from the *P*-helical *Z*-isomer of azoheteroarene BMID. Hopping through the *M*-helical S_1/S_0 conical intersection is presented by red bars, while that through the *P*-helical S_1/S_0 conical intersection is shown by blue bars. Population decay with the derivative of the S_0 population is shown in the insets.

The above helicity preference can be seen more clearly in Fig. 2(a), which presents the distribution of two dihedral angles (C2N3N4C5 and N3N4C5N6, as defined in Scheme 1) at the $S_1 \rightarrow S_0$ hopping points of all 764 trajectories. The distributions of the other geometrical parameters are shown in Fig. S2 (see the ESI†). As can be seen, only two trajectories decayed through the *P*-helical channel, while the other 762 $S_1 \rightarrow S_0$ de-excitations maintained their initial *M*-helicity. So the rate of unidirectional rotation in the *Z*–*E* photoisomerization of BMID was up to 99.7%. This stereospecific excited-state decay was much more obvious than that for *cis*(*Z*)-azobenzene[35] (*ca.* 77% *vs.* 22%) reported by Weingart *et al.*,[35] and even more evident than that of the *cis*(*Z*)-isomer of arylazopyrazole 1,3,5-trimethyl-4-(phenyldiazenyl)-1*H*-pyrazole (*ca.* 97% *vs.* 3%) stated by Wang *et al.*[44]

Based on the 764 hopping geometries shown in Fig. 2(a), two optimized S_1/S_0 conical intersections were located by the

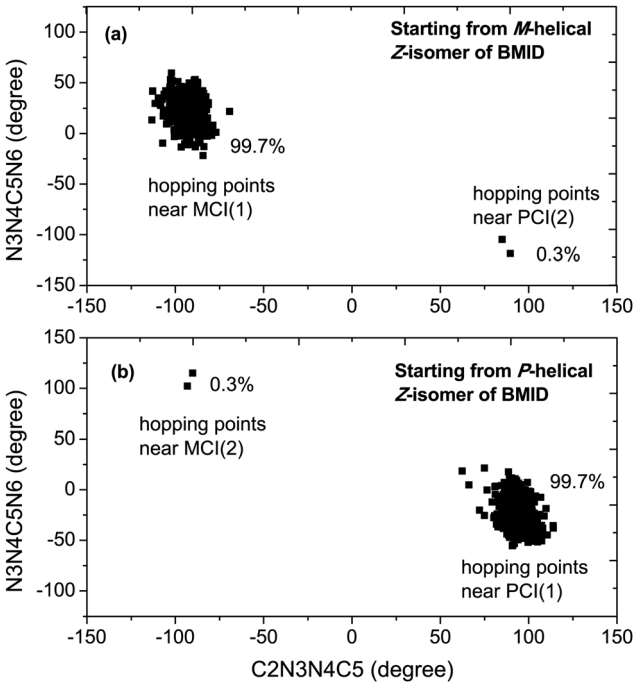

Fig. 2 Distribution of the C2N3N4C5 and N3N4C5N6 dihedral angles at the hopping points of (a) 764 trajectories starting from the *M*-helical *Z*-isomer of azoheteroarene BMID and (b) 694 trajectories starting from the *P*-helical *Z*-isomer of azoheteroarene BMID.

Lagrange-Newton[67] approach, which are presented in Fig. 3(a) and (d) respectively. The enantiomers of the two optimized S_1/S_0 conical intersections were also S_1/S_0 conical intersections, which are shown in Fig. 3(b) and (c), respectively. Owing to the possible rotation around the CN bond (*e.g.*, N4C5) during photoisomerization, both the *M*-helical and *P*-helical S_1/S_0 conical intersections exhibited two different structures. According to their helicities, the four conical intersections in Fig. 3 were named MCI(1), PCI(1), MCI(2) and PCI(2), respectively.

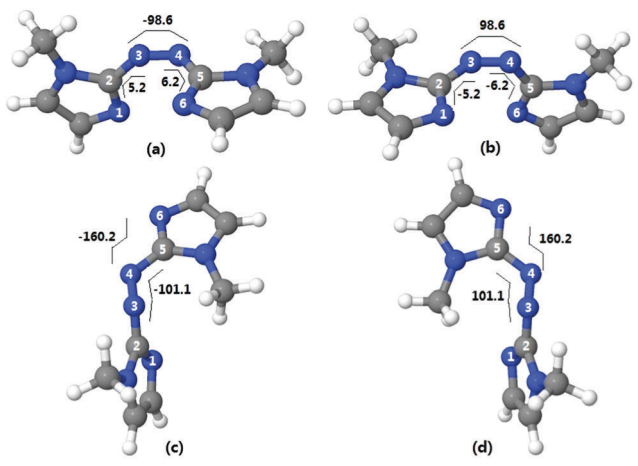

Fig. 3 Optimized geometries of four S_1/S_0 conical intersections for azoheteroarene BMID, calculated with the OM2/MRCI method. According to helicity, they are named (a) MCI(1), (b) PCI(1), (c) MCI(2) and (d) PCI(2), respectively.

The Cartesian coordinates of the conical intersections can be found in the fourth part of the ESI.† The central dihedral angles C2N3N4C5 in MCI(1) and PCI(1) were −98.6° and 98.6°, respectively, while those of MCI(2) and PCI(2) were −101.1° and 101.1°, respectively. We should emphasize that in the 764 trajectories starting from the *M*-helical *Z*-isomer of azoheteroarene BMID, as can be seen in Fig. 2(a), 762 trajectories decayed around MCI(1), while only two trajectories decayed around PCI(2). No trajectories decayed around PCI(1) and MCI(2) in our calculations.

The helicity preference of *Z*–*E* isomerization of BMID, as shown in Fig. 1(a) and 2(a), can be well understood by the reaction paths generated by the linear interpolation between the initial *M*-helical Franck–Condon (MFC) geometry and the relevant S_1/S_0 conical intersections. The energy profiles along different reaction paths for BMID are shown in Fig. 4. For comparison, the energy profiles along different reaction paths for the *Z*–*E* isomerization of azobenzene are also presented, which were calculated with the OM2/MRCI method in the same active space as Weingart *et al.*[35] As shown in Fig. 4, the energies of BMID and azobenzene were relative to the S_1 excited-state energy of the Franck–Condon geometry of their respective *M*-helical *Z*-isomer. As can be seen, the reaction path from MFC to MCI(1) was barrierless and much steeper than that of azobenzene. This was proposed to be the reason why the average lifetime of the S_1 excited state (*ca.* 54 fs) of the *M*-helical *Z*-isomer azoheteroarene BMID was shorter than that of *cis*(*Z*)-azobenzene (*ca.* 72 fs).[35] There is a barrier with a value of 3.48 kcal mol^{-1} along the reaction path from MFC to PCI(2), which is much larger than that of azobenzene (0.03 kcal mol^{-1})[35]

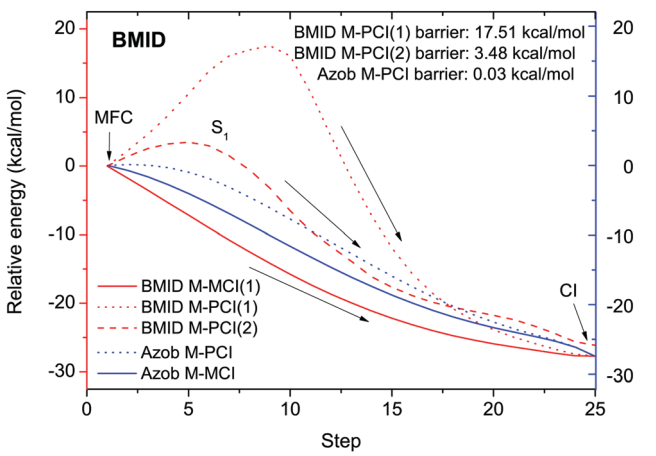

Fig. 4 OM2/MRCI energy profiles along three paths for azoheteroarene BMID (red lines, left), generated by linear interpolation between the Franck–Condon geometry of the *M*-helical *Z*-isomer (MFC) and three different S_1/S_0 conical intersections (MCI(1), PCI(1) and PCI(2)). The energies of BMID are relative to the S_1 excited-state energy of the Franck–Condon geometry of its *M*-helical *Z*-isomer. For comparison, the OM2/MRCI energy profiles for the *M*-helical *Z*-isomer azobenzene (Azob) connecting MFC and two S_1/S_0 conical intersections (MCI and PCI) are also presented, which were calculated with OM2/MRCI in the same active space as Weingart *et al.*[35] The energies of azobenzene are relative to the S_1 excited-state OM2/MRCI energy of the Franck–Condon geometry of its *M*-helical *Z*-isomer.

and also larger than that of 1,3,5-trimethyl-4-(phenyldiazenyl)-1*H*-pyrazole (0.51 kcal mol^{-1}) studied by Wang *et al.*[44] This was proposed to contribute to the significant stereospecific excited-state relaxation in azoheteroarene BMID. We also plotted the reaction path between MFC and PCI(1), as shown in Fig. 4, together with the reaction path between MFC and MCI(2), as shown in Fig. S3 (see the ESI†). As can be seen, the barriers along these two reaction paths were 17.51 kcal mol^{-1} and 52.48 kcal mol^{-1}, respectively. As a result of these high barriers, the trajectories decaying around PCI(1) and MCI(2) were not observed in our calculations.

For the 762 of 764 trajectories de-exciting through the *M*-helical CI, the average S_1 lifetime was approximately 53.6 fs, which was much shorter than the average lifetime (about 89.0 fs) of the two other trajectories through the *P*-helical CI (PCI(2)). This finding was also consistent with the fact that the energy barrier along the MFC-to-PCI(2) reaction path (as shown in Fig. 4) significantly delayed the *Z*–*E* reaction dynamics.

In order to study the effect of the initial helicity, 694 trajectories starting from the S_1 excited state of the *P*-helical *Z*-isomer of azoheteroarene BMID were also calculated for 300 fs. A total of 328 of the 694 trajectories experienced the *E*-isomer structure, so the quantum yield was estimated to be approximately 47% in our calculations. The distribution of the $S_1 \rightarrow S_0$ hopping times of all 694 trajectories starting from the S_1 excited state of the *P*-helical *Z*-isomer of azoheteroarene BMID is presented in Fig. 1(b), together with the population decay and the derivative of the S_0 population shown in the insets. As we can see, the hopping time distributions and population decay curves in Fig. 1(b) are both very similar to those in Fig. 1(a). Almost all trajectories decayed through the channels maintaining their initial *P*-helicity.

The distribution of the dihedral angles C2N3N4C5 and N3N4C5N6 at the $S_1 \rightarrow S_0$ hopping points of all 694 trajectories are shown in Fig. 2(b). The distributions of the other geometrical parameters at the $S_1 \rightarrow S_0$ hopping points are presented in Fig. S4 (see the ESI†). As can be seen, only two trajectories decayed through the *M*-helical channel, while the other 692 $S_1 \rightarrow S_0$ decays maintained their initial *P*-helicity. Therefore, the rate of unidirectional rotation in the *Z*–*E* photoisomerization of azoheteroarene BMID from the *P*-helical structure was also up to 99.7%.

Let us summarize the results presented above. Starting from the S_1 excited state of either the *M*-helical or *P*-helical *Z*-isomer of azoheteroarene BMID, approximately 99.7% trajectories decayed to the ground state through the channel maintaining their initial helicities.

3.2 *Z*–*E* photoisomerization of azoheteroarene BHID

To further clarify the effect of the methyl group on the unidirectional rotation in BMID, we replaced the two methyl groups in BMID with two hydrogen atoms. The new azoheteroarene 1,2-bis(1*H*-imidazol-2-yl)diazene is named BHID for short hereinafter. The optimized geometries of the *M*-helical *Z*-isomer and planar *E*-isomer of BHID calculated with the OM2/MRCI method are displayed in Fig. S5 (see the ESI†), and the corresponding geometrical parameters are summarized in Table S3 (see the ESI†). For comparison, the geometrical parameters calculated with B3LYP/6-311G(d,p) and CAM-B3LYP/6-311G(d,p) using the GAUSSIAN 03 software package[66] are also presented in Table S3 (ESI†). As can be seen, the geometrical parameters of BHID obtained from OM2/MRCI agreed well with those obtained from the density-functional calculations.

On the basis of 649 trajectories starting from the S_1 excited state of the *M*-helical *Z*-isomer, the quantum yield of the *Z*–*E* photoisomerization of azoheteroarene BHID was estimated to be approximately 56%, which was more or less similar to that of azobenzene, and a little larger than that of the above azoheteroarene BMID.

The distribution of the $S_1 \rightarrow S_0$ hopping times for all 649 trajectories starting from the *M*-helical *Z*-isomer of azoheteroarene BHID is presented in Fig. 5(a). Hopping through the *M*-helical S_1/S_0 conical intersection is presented by red bars, while that through the *P*-helical S_1/S_0 conical intersection is shown by blue bars. Population decay together with the derivative of the S_0 population is shown in the insets. As we can see, almost all of the $S_1 \rightarrow S_0$ hopping occurred through the *M*-helical conical intersections, which exhibited the same

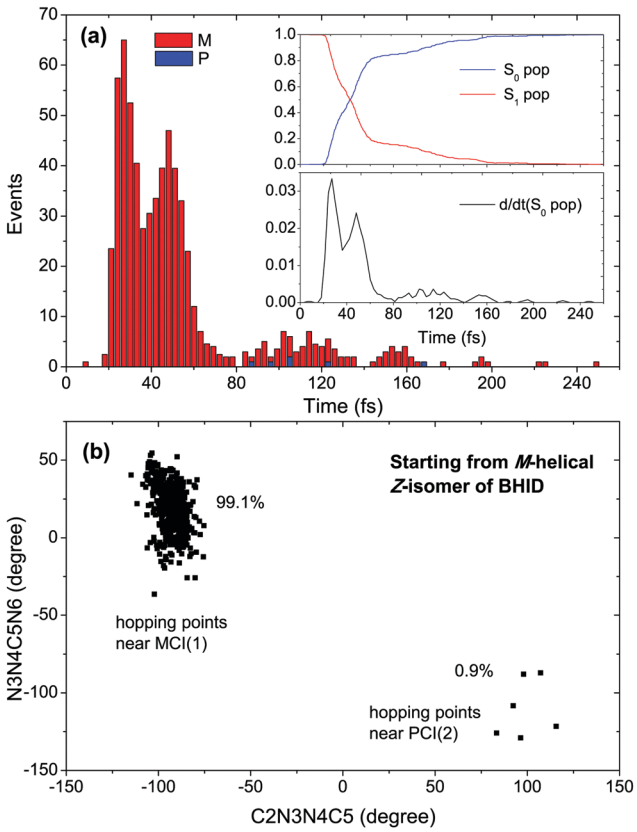

Fig. 5 (a) Distribution of $S_1 \rightarrow S_0$ hopping times for all 649 trajectories starting from the *M*-helical *Z*-isomer of azoheteroarene BHID. Hopping through the *M*-helical S_1/S_0 conical intersection is presented by red bars, while that through the *P*-helical S_1/S_0 conical intersection is shown by blue bars. Population decay with the derivative of the S_0 population is shown in the insets. (b) Distribution of the C2N3N4C5 and N3N4C5N6 dihedral angles at the hopping points of azoheteroarene BHID.

Table 1 Comparison of average S_1 lifetime, quantum yield and chiral path selectivity for the *Z*–*E* photoisomerization of BMID, BHID, azobenzene[a] and 1,3,5-trimethyl-4-(phenyldiazenyl)-1*H*-pyrazole[b] (shortened as Z11 according to Wang *et al.*[44]). M or P in parentheses represents helicity of the molecule

	BMID(M)	BMID(P)	BHID(M)	Azobenzene(P)[a]	Z11(M)[b]	Z11(P)[b]
Average S_1 lifetime	54 fs	55 fs	50 fs	72 fs	49 fs	52 fs
Quantum yield (ϕ_{Z-E})	47%	47%	56%	58%	52%	51%
Chiral path preference	99.7% *vs.* 0.3%	99.7% *vs.* 0.3%	99.1% *vs.* 0.9%	77.3% *vs.* 22.3%	97% *vs.* 3%	97% *vs.* 3%

[a] Results from ref. 35 [b] Results from ref. 44

helicity as their initial geometries, and only a very few trajectories decayed through the *P*-helical conical intersection. Similar to azoheteroarene BMID, the S_1 population decay of the *Z*-isomer azoheteroarene BHID was obviously not exponential, but exhibited an oscillatory pattern. Two decay maxima occurred before 60 fs, at approximately 27 fs and 48 fs, respectively.

The distribution of the dihedral angles C2N3N4C5 and N3N4C5N6 at the $S_1 \rightarrow S_0$ hopping points of all 649 trajectories is shown in Fig. 5(b). The distributions of the other geometrical parameters are displayed in Fig. S6 (see the ESI†). As we can see, only 6 trajectories decayed through the *P*-helical conical intersections, while the other 643 trajectories decayed through the *M*-helical conical intersections. Therefore, the rate of unidirectional rotation for the *Z*–*E* isomerization of azoheteroarene BHID was up to 99.1%.

The discussion on the S_1/S_0 conical intersections responsible for the *Z*–*E* isomerization of azoheteroarene BHID is presented in the seventh part of the ESI.† Similar to BMID, the rather high chiral selectivity in the *Z*–*E* photoisomerization of BHID can be well understood by examining the linear-interpolated reaction paths connecting the initial *M*-helical Franck–Condon geometry and the relevant S_1/S_0 conical intersections. A detailed discussion is presented in the eighth part of the ESI.†

As we can see, no obvious substituent effect on the photoisomerization dynamics was observed between BMID and BHID, that is, different substituents for these azoheteroarene-based compounds did not change the unidirectional excited-state torsional mechanism.

The average lifetime of the S_1 excited state, quantum yield and chiral path preference rate for the *Z*–*E* isomerization of azoheteroarene BMID, BHID, azobenzene[35] and 1,3,5-trimethyl-4-(phenyldiazenyl)-1*H*-pyrazole[44] are summarized in Table 1 for comparison. As we can see, azoheteroarene BMID, BHID and 1,3,5-trimethyl-4-(phenyldiazenyl)-1*H*-pyrazole exhibited similar average S_1 excited state lifetimes, which were a little shorter than that of azobenzene. The quantum yields of *Z*–*E* photoisomerization were similar for all compounds. Azoheteroarene BMID and BHID exhibited a more obvious chiral path preference than their counterparts azobenzene and 1,3,5-trimethyl-4-(phenyldiazenyl)-1*H*-pyrazole.

4 Conclusions

Using trajectory surface-hopping molecular dynamics at the semi-empirical OM2/MRCI level, the *Z*–*E* photoisomerization dynamics of two azoheteroarenes, 1,2-bis(1-methyl-1*H*-imidazol-2-yl)diazene and 1,2-bis(1*H*-imidazol-2-yl)diazene, which were induced by nπ* excitation, are investigated in detail.

Based on a large number of trajectories starting from the S_1 excited state of the *Z*-isomer, for both azoheteroarenes, more than 99% of the trajectories decayed to their ground states through conical intersections with the same helicities as their initial geometries, that is, stereospecific unidirectional excited-state relaxations were found. This chiral path preference could be well understood by the energy profiles generated by linear interpolation between the Franck–Condon geometry of the *Z*-isomer and the relevant S_1/S_0 conical intersections. The average lifetimes of the S_1 excited state for both azoheteroarenes in our calculations were approximately 50 fs, a little shorter than that of azobenzene (*ca.* 72 fs). The quantum yields of the *Z*–*E* photoisomerization for both azoheteroarenes were a little smaller than that of azobenzene, but still large enough to be an effective photoswitch. Except for the more obvious chiral path preference, we found that the photoisomerization mechanism of these two azoheteroarenes was similar to their counterpart azobenzene. Since different substituents for these azoheteroarene-based compounds do not change their unidirectional excited-state torsional mechanism, from a general perspective, our theoretical results may provide a step towards the design of novel ultrafast optical switching devices in the near future.

Conflicts of interest

There are no conflicts to declare.

Acknowledgements

This work was supported by the National Natural Science Foundation of China (Grant 11534008, 21203144, 21673266, 21543008 and 11504288), the Doctoral Fund of Ministry of Education of China (Grant 20120201120056), the Fundamental Research Funds for the Central Universities (xjj2016053) and the HPC Platform in Xi'an Jiaotong University. C. J. thanks Prof. G. Cui for discussion and the financial support from the China Scholarship Council. Z. L. acknowledges the support from Distinguished Young Scholars (JQ201504) from the Natural Science Foundation of Shandong Province.

References

1 D. Gegiou, K. A. Muszkat and E. Fisher, *J. Am. Chem. Soc.*, 1968, **90**, 12.

2 P. Bortolus and S. Monti, *J. Phys. Chem.*, 1979, **83**, 648.
3 H. Rau and E. Lüddecke, *J. Am. Chem. Soc.*, 1982, **104**, 1616.
4 H. Rau, in *Photochromism: Molecules and Systems*, ed. H. Dürr and H. Bouas-Laurent, Elsevier, Amsterdam, 1990, ch. 4, p. 165.
5 H. Rau, *J. Photochem.*, 1984, **26**, 221.
6 I. K. Lednev, T. Q. Ye, L. C. Abbott, R. E. Hester and J. N. Moore, *J. Phys. Chem. A*, 1998, **102**, 9161.
7 T. Fujino and T. Tahara, *J. Phys. Chem. A*, 2000, **104**, 4203.
8 H. Satzger, S. Spörlein, C. Root, J. Wachtveiti, W. Zinth and P. Gilch, *Chem. Phys. Lett.*, 2003, **372**, 216.
9 M. S. Scholz, J. N. Bull, N. J. A. Coughlan, E. Carrascosa, B. D. Adamson and E. J. Bieske, *J. Phys. Chem. A*, 2017, **121**, 6413.
10 T. Pancur, F. Renth, F. Temps, B. Harbaum, A. Krüger, R. Hergesb and C. Näther, *Phys. Chem. Chem. Phys.*, 2005, **7**, 1985.
11 Y. Norikane and N. Tamaoki, *Eur. J. Org. Chem.*, 2006, 1296.
12 K. Janus and J. Sworakowski, *J. Phys. Chem. B*, 2005, **109**, 93.
13 G. Haberhauer and C. Kallweit, *Angew. Chem., Int. Ed.*, 2010, **49**, 2418.
14 R. Siewertsen, H. Neumann, B. Buchheim-Stehn, R. Herges, C. Näther, F. Renth and F. Temps, *J. Am. Chem. Soc.*, 2009, **131**, 15594.
15 A. A. Beharry, O. Sadovski and G. A. Woolley, *J. Am. Chem. Soc.*, 2011, **133**, 19684.
16 D. Bléger, J. Schwarz, A. M. Brouwer and S. Hecht, *J. Am. Chem. Soc.*, 2012, **134**, 20597.
17 Y. Yang, R. P. Hughes and I. Aprahamian, *J. Am. Chem. Soc.*, 2012, **134**, 15221.
18 T. Ishikawa, T. Noro and T. Shoda, *J. Chem. Phys.*, 2001, **115**, 7503.
19 A. Cembran, F. Bernardi, M. Garavelli, L. Gagliardi and G. Oriandi, *J. Am. Chem. Soc.*, 2004, **126**, 3234.
20 E. W.-G. Diau, *J. Phys. Chem. A*, 2004, **108**, 950.
21 C. Ciminelli, G. Granucci and M. Persico, *Chem. – Eur. J.*, 2004, **10**, 2327.
22 I. Conti, M. Garavelli and G. Orlandi, *J. Am. Chem. Soc.*, 2008, **130**, 5216.
23 M. L. Tiago, S. Ismail-Beigi and S. G. Louie, *J. Chem. Phys.*, 2005, **122**, 094311.
24 A. Toniolo, C. Ciminelli, M. Persico and T. J. Martinez, *J. Chem. Phys.*, 2005, **123**, 234308.
25 P. Sauer and R. E. Allen, *Chem. Phys. Lett.*, 2008, **450**, 192.
26 Y. Ootani, K. Satoh, A. Nakayama, T. Noro and T. Taketsugu, *J. Chem. Phys.*, 2009, **131**, 194306.
27 J. Shao, Y. Lei, Z. Wen, Y. Dou and Z. Wang, *J. Chem. Phys.*, 2008, **129**, 164111.
28 S. Yuan, Y. Dou, W. Wu, Y. Hu and J. Zhao, *J. Phys. Chem. A*, 2008, **112**, 13326.
29 C. Jiang, R. Xie, F. Li and R. E. Allen, *J. Phys. Chem. A*, 2011, **115**, 244.
30 C. Jiang, R. Xie, F. Li and R. E. Allen, *Chem. Phys. Lett.*, 2012, **521**, 107.
31 M. Pederzoli, J. Pittner, M. Barbatti and H. Lischka, *J. Phys. Chem. A*, 2011, **115**, 11136.
32 T. Cusati, G. Granucci and M. Persico, *J. Am. Chem. Soc.*, 2011, **133**, 5109.
33 M. Böockmann, N. Doltsinis and D. Marx, *J. Phys. Chem. A*, 2009, **114**, 745.
34 M. Böckmann, N. L. Doltsinis and D. Marx, *Angew. Chem., Int. Ed.*, 2010, **49**, 3382.
35 O. Weingart, Z. Lan, A. Koslowski and W. Thiel, *J. Phys. Chem. Lett.*, 2011, **2**, 1506.
36 J. Góamez, O. Weingart, A. Koslowski and W. Thiel, *J. Chem. Theory Comput.*, 2012, **8**, 2352–2358.
37 M. Moreno, R. Gelabert and J. M. Lluch, *ChemPhysChem*, 2016, **17**, 2824.
38 J. Casellas, M. J. Bearpark and M. Reguero, *ChemPhysChem*, 2016, **17**, 3068.
39 W. Gao, L. Yu, X. Zheng, Y. Lei, C. Zhu and H. Han, *RSC Adv.*, 2016, **6**, 39542.
40 L. Yue, L. Yu, C. Xu, Y. Lei, Y. Liu and C. Zhu, *ChemPhysChem*, 2017, **18**, 1274.
41 C. E. Weston, R. D. Richardson, P. Haycock, A. White and M. J. Fuchter, *J. Am. Chem. Soc.*, 2014, **136**, 11878.
42 J. Calbo, C. E. Weston, A. J. P. White, H. S. Raepa, J. Contreras-Garcia and M. J. Fuchter, *J. Am. Chem. Soc.*, 2017, **139**, 1261.
43 T. Yin, Z. Zhao and H. Zhang, *New J. Chem.*, 2017, **41**, 1659.
44 Y. Wang, X. Liu, G. Cui, W. Fang and W. Thiel, *Angew. Chem., Int. Ed.*, 2016, **55**, 14009.
45 C. E. Weston, R. D. Richardson and M. J. Fuchter, *Chem. Commun.*, 2016, **52**, 4521.
46 C. E. Weston, A. Kramer, F. Colin, O. Yildiz, M. G. J. Baud, F. Meyer-Almes and M. J. Fuchter, *ACS Infect. Dis.*, 2017, **3**, 152.
47 K. Ghebreyessus and S. M. Cooper Jr., *Organometallics*, 2017, **36**, 3360.
48 A. S. Lyakhov, T. V. Serebryanskaya, P. N. Gaponik, S. V. Voitekhovich and L. S. Ivashkevich, *Acta Crystallogr.*, 2006, **C62**, m223.
49 B. L. Feringa, *Acc. Chem. Res.*, 2001, **34**, 504.
50 B. L. Feringa, *J. Org. Chem.*, 2007, **72**, 6635.
51 N. Koumura, R. W. J. Zijlstra, R. A. van Delden, N. Harada and B. L. Feringa, *Nature*, 1999, **401**, 152.
52 G. Marchand, J. Eng, I. Schapiro, A. Valentini, L. M. Frutos, E. Pieri, M. Olivucci, J. Leonard and E. Gindensperger, *J. Phys. Chem. Lett.*, 2015, **6**, 599.
53 C. Zhu and H. Nakamura, *J. Chem. Phys.*, 1992, **97**, 8497.
54 C. Zhu and H. Nakamura, *J. Chem. Phys.*, 1993, **98**, 6208.
55 W. Thiel, *MNDO program, version 6.1*, Max-Planck-Institut fur Kohlenforschung, Mulheim, 2007.
56 W. Weber and W. Thiel, *Theor. Chem. Acc.*, 2000, **103**, 495.
57 N. Otte, M. Scholten and W. Thiel, *J. Phys. Chem. A*, 2007, **111**, 5751.
58 X. Zhuang, J. Wang and Z. Lan, *J. Phys. Chem. A*, 2013, **117**, 4785.
59 P. O. Dral, X. Wu, L. Spörkel, A. Koslowski, W. Weber, R. Steiger, M. Scholten and W. Theil, *J. Chem. Theory Comput.*, 2016, **12**, 1082.
60 P. O. Dral, X. Wu, L. Spörkel, A. Koslowski and W. Theil, *J. Chem. Theory Comput.*, 2016, **12**, 1097.
61 D. Tuna, Y. Lu, A. Koslowski and W. Theil, *J. Chem. Theory Comput.*, 2016, **12**, 4400.

62 H. Berit, Z. Lan and W. Thiel, *Phys. Chem. Chem. Phys.*, 2012, **14**, 8137.
63 S. Xia, B. Xie, Q. Fang, G. Cui and W. Thiel, *Phys. Chem. Chem. Phys.*, 2015, **17**, 9687.
64 X. Pang, X. Cui, D. Hu, C. Jiang, D. Zhao, Z. Lan and F. Li, *J. Phys. Chem. A*, 2017, **121**, 1240.
65 D. Hu, J. Huang, Y. Xie, L. Yue, X. Zhuang and Z. Lan, *Chem. Phys.*, 2015, **463**, 95.
66 M. J. Frisch, G. W. Trucks, H. B. Schlegel, G. E. Scuseria, M. A. Robb, J. R. Cheeseman, J. A. Montgomery, Jr., T. Vreven, K. N. Kudin, J. C. Burant, J. M. Millam, S. S. Iyengar, J. Tomasi, V. Barone, B. Mennucci, M. Cossi, G. Scalmani, N. Rega, G. A. Petersson, H. Nakatsuji, M. Hada, M. Ehara, K. Toyota, R. Fukuda, J. Hasegawa, M. Ishida, T. Nakajima, Y. Honda, O. Kitao, H. Nakai, M. Klene, X. Li, J. E. Knox, H. P. Hratchian, J. B. Cross, V. Bakken, C. Adamo, J. Jaramillo, R. Gomperts, R. E. Stratmann, O. Yazyev, A. J. Austin, R. Cammi, C. Pomelli, J. W. Ochterski, P. Y. Ayala, K. Morokuma, G. A. Voth, P. Salvador, J. J. Dannenberg, V. G. Zakrzewski, S. Dapprich, A. D. Daniels, M. C. Strain, O. Farkas, D. K. Malick, A. D. Rabuck, K. Raghavachari, J. B. Foresman, J. V. Ortiz, Q. Cui, A. G. Baboul, S. Clifford, J. Cioslowski, B. B. Stefanov, G. Liu, A. Liashenko, P. Piskorz, I. Komaromi, R. L. Martin, D. J. Fox, T. Keith, M. A. Al-Laham, C. Y. Peng, A. Nanayakkara, M. Challacombe, P. M. W. Gill, B. Johnson, W. Chen, M. W. Wong, C. Gonzalez and J. A. Pople,*Gaussian 03, Revision C.02*, Gaussian, Inc., Wallingford CT, 2004.
67 T. W. Keal, A. Koslowski and W. Thiel, *Theor. Chem. Acc.*, 2007, **118**, 837.
68 J. C. Tully, *J. Chem. Phys.*, 1990, **93**, 1061.
69 S. H. Schiffer and J. C. Tully, *J. Chem. Phys.*, 1994, **101**, 4657.
70 E. Fabiano, G. Groenhof and W. Thiel, *Chem. Phys.*, 2008, **351**, 111.
71 G. Granucci, M. Persico and A. Zoccante, *J. Chem. Phys.*, 2010, **133**, 134111.
72 M. Barbatti, G. Granucci, M. Persico, M. Ruckenbauer, M. Vazdar, M. Eckert-Maksic and H. Lischka, *J. Photochem. Photobiol., A*, 2007, **190**, 228.